nature medicine

# LIFR is a breast cancer metastasis suppressor upstream of the Hippo-YAP pathway and a prognostic marker

Dahu Chen[1], Yutong Sun[2,8], Yongkun Wei[2,8], Peijing Zhang[1], Abdol Hossein Rezaeian[2], Julie Teruya-Feldstein[3], Sumeet Gupta[4], Han Liang[5], Hui-Kuan Lin[2,6], Mien-Chie Hung[2,6,7] & Li Ma[1,6]

**There is a pressing need to identify prognostic markers of metastatic disease and targets for treatment. Combining high-throughput RNA sequencing, functional characterization, mechanistic studies and clinical validation, we identify leukemia inhibitory factor receptor (LIFR) as a breast cancer metastasis suppressor downstream of the microRNA miR-9 and upstream of Hippo signaling. Restoring LIFR expression in highly malignant tumor cells suppresses metastasis by triggering a Hippo kinase cascade that leads to phosphorylation, cytoplasmic retention and functional inactivation of the transcriptional coactivator YES-associated protein (YAP). Conversely, loss of LIFR in nonmetastatic breast cancer cells induces migration, invasion and metastatic colonization through activation of YAP. LIFR is downregulated in human breast carcinomas and inversely correlates with metastasis. Notably, in approximately 1,000 nonmetastatic breast tumors, LIFR expression status correlated with metastasis-free, recurrence-free and overall survival outcomes in the patients. These findings identify LIFR as a metastasis suppressor that functions through the Hippo-YAP pathway and has significant prognostic power.**





Breast cancer begins as a local disease and can metastasize to the lymph nodes and other organs[1,2]. Surgery, chemotherapy and radiation therapy can control many localized tumors, but the overall utility of these treatment methods in restricting the development of metastasis and treating metastatic disease is limited[3]. New technologies have led to the identification of molecules that contribute to the development of metastasis. Thus far, a plethora of metastasis promoters have been identified and intensively characterized; however, relatively few genes have been established as metastasis suppressors[4,5].

Tumor initiation and progression can be regulated by microRNAs (miRNAs), which are endogenously expressed small noncoding RNAs that cause degradation of target mRNAs, inhibition of the translation of these mRNAs or both[6–8]. We and others have previously shown the existence of metastasis-promoting and metastasis-suppressing miRNAs[9–15], including miR-9, which targets E-cadherin and promotes the metastasis of breast carcinoma cells expressing this cell-adhesion molecule[14].

In this study, we investigated E-cadherin–independent functions of miR-9 and identified *LIFR* as a miR-9 target in E-cadherin–negative tumor cells and a new metastasis suppressor. Mechanistically, LIFR inhibits metastasis through the Hippo-YAP pathway. In human breast cancer, loss of LIFR is associated with poor prognosis.

## RESULTS

### *LIFR* is a direct and functional target of miR-9

miR-9 can promote metastasis by targeting the metastasis suppressor E-cadherin[14]. Downregulation or loss of E-cadherin has been implicated in human tumors[16,17]. To determine whether miR-9 regulates the metastasis of breast cancer cells that have lost E-cadherin, we stably expressed miR-9 in the E-cadherin–negative, nonmetastatic human breast cancer cell line SUM159 (ref. 14) and implanted these GFP-labeled cells into the mammary fat pads of female nonobese diabetic severe combined immunodeficient (NOD-SCID) mice. We euthanized all recipient mice at 12 weeks after implantation and found no significant difference ($P = 0.4$) in the weights of the primary mammary tumors formed by miR-9–expressing SUM159 cells compared to those formed by mock-infected (control) SUM159 cells (**Supplementary Fig. 1a**). Hosts of the control tumors had no detectable metastases; in contrast, mice bearing miR-9–expressing tumors had lung, kidney, adrenal and peritoneal metastases (**Supplementary Fig. 1b–d**). Thus, miR-9 can function as a metastasis-promoting miRNA in E-cadherin–negative breast cancer cells.

To determine the mechanisms by which miR-9 promotes metastasis in E-cadherin–negative cancer cells, we performed a high-throughput RNA sequencing analysis and identified 503 genes whose expression was more than 1.5 times higher in mock-infected cells than in miR-9–expressing SUM159 cells (**Supplementary Table 1**). Of these

[1]Department of Experimental Radiation Oncology, The University of Texas MD Anderson Cancer Center, Houston, Texas, USA. [2]Department of Molecular and Cellular Oncology, The University of Texas MD Anderson Cancer Center, Houston, Texas, USA. [3]Department of Pathology, Memorial Sloan-Kettering Cancer Center, New York, New York, USA. [4]Whitehead Institute for Biomedical Research, Cambridge, Massachusetts, USA. [5]Department of Bioinformatics and Computational Biology, The University of Texas MD Anderson Cancer Center, Houston, Texas, USA. [6]Cancer Biology Program, Graduate School of Biomedical Sciences, The University of Texas Health Science Center at Houston, Houston, Texas, USA. [7]Center for Molecular Medicine and Graduate Institute of Cancer Biology, China Medical University, Taichung, Taiwan. [8]These authors contributed equally to this work. Correspondence should be addressed to L.M. (lma4@mdanderson.org).

Received 12 March; accepted 15 August; published online 23 September 2012; doi:10.1038/nm.2940

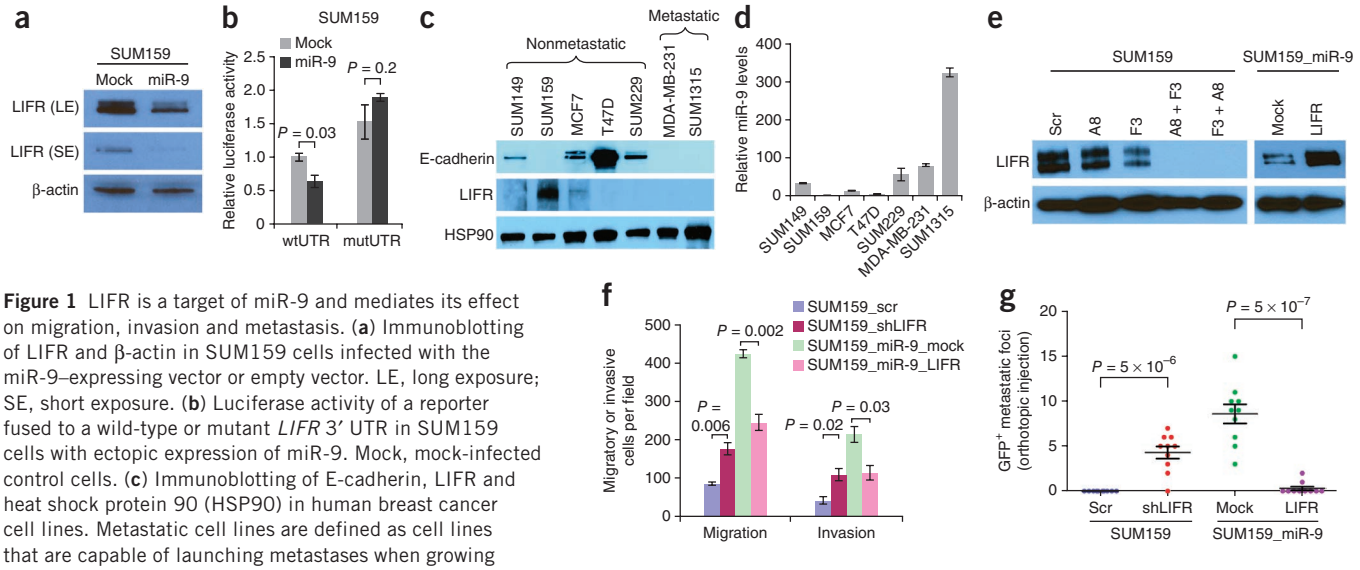


**Figure 1** LIFR is a target of miR-9 and mediates its effect on migration, invasion and metastasis. (**a**) Immunoblotting of LIFR and β-actin in SUM159 cells infected with the miR-9–expressing vector or empty vector. LE, long exposure; SE, short exposure. (**b**) Luciferase activity of a reporter fused to a wild-type or mutant *LIFR* 3′ UTR in SUM159 cells with ectopic expression of miR-9. Mock, mock-infected control cells. (**c**) Immunoblotting of E-cadherin, LIFR and heat shock protein 90 (HSP90) in human breast cancer cell lines. Metastatic cell lines are defined as cell lines that are capable of launching metastases when growing as primary tumors in mice. (**d**) Quantitative PCR (qPCR) of miR-9 in the same cell lines used in **c**. (**e**) Immunoblotting of LIFR and β-actin in SUM159 cells infected with LIFR shRNA (clones A8 and F3, alone or in combination) and in miR-9–overexpressing SUM159 cells (SUM159_miR-9) infected with human LIFR. Scr, the pGIPZ-GFP lentiviral vector with a scrambled sequence that does not target any mRNA. (**f**) Transwell migration and Matrigel invasion assays of SUM159 cells infected with LIFR shRNA (shLIFR; clones A8 + F3) and of SUM159_miR-9 cells infected with LIFR. (**g**) Number of GFP-positive foci in the lungs of mice with orthotopic injection of cells described in **f** at week 12 after implantation. ($n$ = 10 mice per group). Statistical significance was determined by unpaired, two-tailed Student's $t$ test. Data are means ± s.e.m.

503 genes, 56 contain the miR-9–binding site in their 3′ untranslated region (UTR) (**Supplementary Table 1**). Oncomine data-mining analyses showed that among these 56 genes, only one, *LIFR*, is consistently downregulated in clinical breast cancers and many other cancer types (**Supplementary Table 2**).

*LIFR* mRNA contains a conserved miR-9–binding site in its 3′ UTR (**Supplementary Fig. 2a**). In SUM159 cells with ectopic miR-9 expression, we found a pronounced reduction in LIFR protein expression compared with mock-infected cells (**Fig. 1a**). In both SUM159 and 293T cells, ectopic expression of miR-9 reduced the activity of a luciferase reporter fused to the wild-type *LIFR* 3′ UTR but not the activity of a reporter fused to a mutant *LIFR* 3′ UTR with mutations in the miR-9 seed-pairing[18] region (**Fig. 1b** and **Supplementary Fig. 2a**,**b**). Thus, the observed downregulation of luciferase activity by miR-9 directly depends on a single binding site in the *LIFR* 3′ UTR.

We then examined the protein expression of LIFR and E-cadherin in human breast cancer cell lines. The nonmetastatic tumor cell lines SUM149, SUM159, MCF7, T47D and SUM229 expressed detectable levels of either E-cadherin or LIFR (**Fig. 1c**). In contrast, the expression of both LIFR and E-cadherin was lost in the metastatic cell lines MDA-MB-231 and SUM1315 (**Fig. 1c**), which had the highest expression of miR-9 of all the cell lines examined (**Fig. 1d**). Thus, in these breast cancer cell lines, concomitant loss of LIFR and E-cadherin is associated with miR-9 expression and metastatic ability.

The function of LIFR in tumor progression and metastasis has not been shown. Hence, we performed both loss-of-function and gain-of-function analyses of LIFR (**Fig. 1e**). Manipulating LIFR expression did not alter cell proliferation or viability *in vitro* (**Supplementary Fig. 3a**,**b**) or the growth of primary mammary tumors *in vivo* (**Supplementary Fig. 3c**). However, silencing LIFR expression in SUM159 cells partially recapitulated the effect of miR-9 overexpression on promoting migration, invasion and metastasis; conversely, restoring LIFR expression in miR-9–overexpressing SUM159 cells reversed the effect of this miRNA (**Fig. 1f**,**g** and **Supplementary Fig. 3d–h**). Therefore, downregulation of LIFR mediates, at least partially, the metastasis-promoting effect of miR-9 in these E-cadherin–negative breast cancer cells.

## Restoring LIFR in malignant cells suppresses metastasis

We next expressed LIFR in the MDA-MB-231 human cell line and the 4T1 mouse cell line (**Supplementary Fig. 4a**,**b**), two naturally metastatic breast cancer cell lines. Whereas 4T1 and MDA-MB-231 cells had low basal expression of *LIFR*, the level of *LIFR* mRNA was more than 200 times higher in normal mouse breast tissue than in 4T1 cells (**Supplementary Fig. 4b**). Ectopic expression of LIFR in these two cell lines did not substantially alter their *in vitro* growth or viability (**Supplementary Fig. 4c**,**d**) but did markedly inhibit cell migration and invasion (**Supplementary Fig. 4e–h**).

We then implanted the infected 4T1 cells into the mammary fat pads of syngeneic BALB/c female mice. At day 25 after implantation, we found a 41% reduction ($P$ = 0.05) in the weight of the primary tumor formed by the LIFR-expressing 4T1 cells (**Supplementary Fig. 5a**). The control (mock-infected) 4T1 tumors were invasive and infiltrated the adjacent adipose tissue, whereas LIFR-expressing 4T1 tumors were confined by a fibrotic capsule and largely noninvasive (**Fig. 2a**). At this time point, mice bearing LIFR-expressing 4T1 tumors had no visible metastases, whereas the hosts of mock-infected 4T1 cells had an average of 3.3 metastatic nodules in the lung (**Fig. 2b–d**). At day 31, most mice in both groups were moribund as a result of large primary tumors, and we found no significant difference ($P$ = 0.6) in the weights of the primary tumors between the two groups (**Supplementary Fig. 5a**). At this time point, mice implanted with mock-infected 4T1 cells had an average of 12.3 visible lung metastases per mouse, whereas mice bearing LIFR-expressing 4T1 tumors had 79% fewer ($P = 6 \times 10^{-4}$) lung metastases, with an average of 2.6 visible metastases per mouse (**Fig. 2b–d**). Therefore, restoring LIFR expression

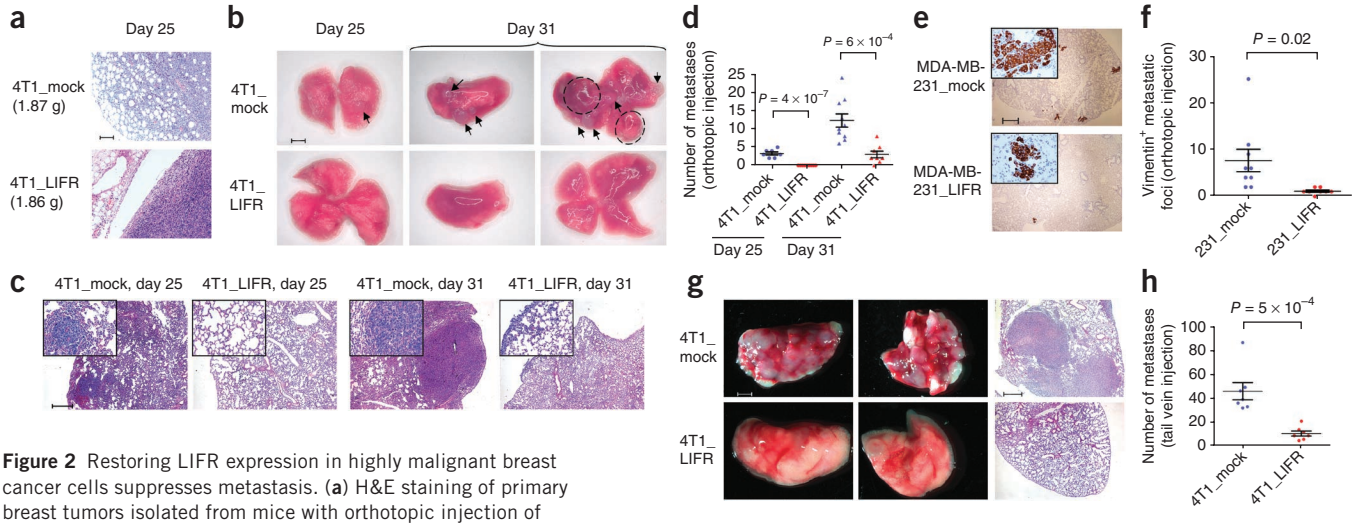


**Figure 2** Restoring LIFR expression in highly malignant breast cancer cells suppresses metastasis. (**a**) H&E staining of primary breast tumors isolated from mice with orthotopic injection of LIFR-transduced 4T1 cells (4T1_LIFR) or mock-infected 4T1 cells (4T1_mock) at day 25 after implantation. Scale bar, 100 μm. The weight of the primary tumor is indicated in parentheses. (**b**,**c**) Bright-field imaging (**b**) and H&E staining (**c**) of lungs isolated from mice with orthotopic injection of LIFR-transduced or mock-infected 4T1 cells at days 25 and 31 after implantation. Scale bars: **b**, 2,000 μm; **c**, 500 μm. Arrows and circles in **b** indicate visible metastatic nodules. Insets in **c** are high-magnification (×200) images of specific areas in the corresponding low-magnification (×25) images. (**d**) Number of metastatic nodules in the lungs of mice with orthotopic injection of LIFR-transduced or mock-infected 4T1 cells at days 25 and 31 after implantation. Data are means ± s.e.m. ($n$ = 7, 9, 10 and 8 mice, respectively, in the four groups shown from left to right). (**e**,**f**) Human-specific vimentin immunohistochemical staining (**e**) and the number of vimentin-positive foci (**f**) in the lungs of mice with orthotopic injection of LIFR-transduced MDA-MB-231 cells (MDA-MB-231_LIFR) or mock-infected MDA-MB-231 cells (MDA-MB-231_mock) at week 10 after implantation. Scale bar, 600 μm. Insets in **e** are high-magnification (×600) images of vimentin-positive foci in the corresponding low-magnification (×40) images. Data in **f** are means ± s.e.m. ($n$ = 9 and 8 mice in the control and LIFR groups, respectively). (**g**,**h**) Bright-field imaging (**g**, left and middle), H&E staining (**g**, right) and the number of metastatic nodules (**h**) in the lungs of mice with tail vein injection of LIFR-transduced or mock-infected 4T1 cells at day 21 after implantation. Scale bar, bright-field images (left and middle), 2,000 μm; H&E staining (right), 500 μm. White nodules in **g** are macroscopic metastases. Data in **h** are means ± s.e.m. ($n$ = 7 mice per group). Statistical significance was determined by unpaired, two-tailed Student's $t$ test.

led to an initial delay in 4T1 tumor growth and a persistent reduction in metastasis formation by otherwise highly malignant cells.

Next, we performed orthotopic implantation of LIFR-expressing or mock-infected MDA-MB-231 cells, which are negative for E-cadherin and positive for vimentin. At 10 weeks after implantation, we found no significant difference ($P$ = 0.45) in primary tumor size between the two groups (**Supplementary Fig. 5b**). As LIFR expression did not substantially alter vimentin expression (**Supplementary Fig. 6a**), we used a human-specific antibody to vimentin to detect metastasis and found that mice bearing LIFR-expressing MDA-MB-231 cells (averaging 1.1 metastatic foci per mouse) had 86% fewer ($P$ = 0.02) vimentin-positive foci in the lung than mice implanted with mock-infected cells (averaging 7.7 metastatic foci per mouse; **Fig. 2e**,**f**).

To determine the effect of LIFR on metastatic colonization, we injected LIFR-expressing 4T1 cells through the tail vein. Compared with mice implanted with the control 4T1 cells (averaging 45.9 visible metastases per mouse), mice that received intravenous injection of LIFR-transduced 4T1 cells showed a 76% reduction ($P = 5 \times 10^{-4}$) in the number of metastatic nodules in the lung, with an average of 10.9 visible metastases per mouse (**Fig. 2g**,**h**). Taken together, these results show that LIFR suppresses both the early (invasion) and late (colonization) steps of metastasis.

## LIFR activates Hippo signaling leading to YAP inactivation

Heterodimerization of LIFR with the glycoprotein gp130 mediates the biological activities of leukemia inhibitory factor (LIF)[19]. Although the signaling pathways downstream of LIFR have not been directly characterized, previous observations of LIF suggested two candidate pathways: (i) treatment with LIF can activate JAK–signal transducer and activator of transcription 3 (STAT3) signaling[20], or (ii) withdrawal of LIF from the medium of cultured mouse embryonic stem cells can increase the phosphorylation of YAP at Ser112 (ref. 21), which is equivalent to Ser127 of human YAP.

Accordingly, we examined whether LIFR affects the phosphorylation of STAT3 and YAP in 4T1 and MDA-MB-231 breast cancer cells. Although LIF treatment did induce STAT3 phosphorylation, this phosphorylation was undetectable in both mock-infected and LIFR-overexpressing cells without LIF stimulation (**Supplementary Fig. 6b**). However, either treatment with LIF or ectopic expression of LIFR increased YAP Ser112 phosphorylation in 4T1 cells and YAP Ser127 phosphorylation in MDA-MB-231 cells (**Fig. 3a**). Conversely, knockdown of LIFR in SUM159 cells resulted in a 65% reduction in YAP Ser127 phosphorylation (**Fig. 3b**). These results contrasted with a recent report in which withdrawal of LIF from mouse embryonic stem cell culture increased YAP phosphorylation[21] (**Supplementary Discussion**).

This phosphorylation causes cytoplasmic sequestration of YAP, thereby preventing its nuclear translocation and function as a transcriptional coactivator[22,23]. Compared with mock-infected 4T1 cells, LIFR-overexpressing 4T1 cells had increased levels of cytoplasmic YAP and reduced levels of nuclear YAP, as gauged by fractionation assays and immunofluorescent staining; conversely, knockdown of LIFR in SUM159 cells promoted the nuclear localization of YAP (**Fig. 3c–f**).

When in the nucleus, YAP interacts with several transcription factors[24]. We determined the mRNA levels of previously reported YAP targets[25,26]: *AREG*, *FGF1*, *BIRC2* and *BIRC5* showed no substantial change as a result of LIFR expression, whereas *BDNF* and *CTGF* mRNA levels both showed a >50% decrease (**Fig. 3g** and **Supplementary Fig. 7**). *GLI2* mRNA was undetectable in both control

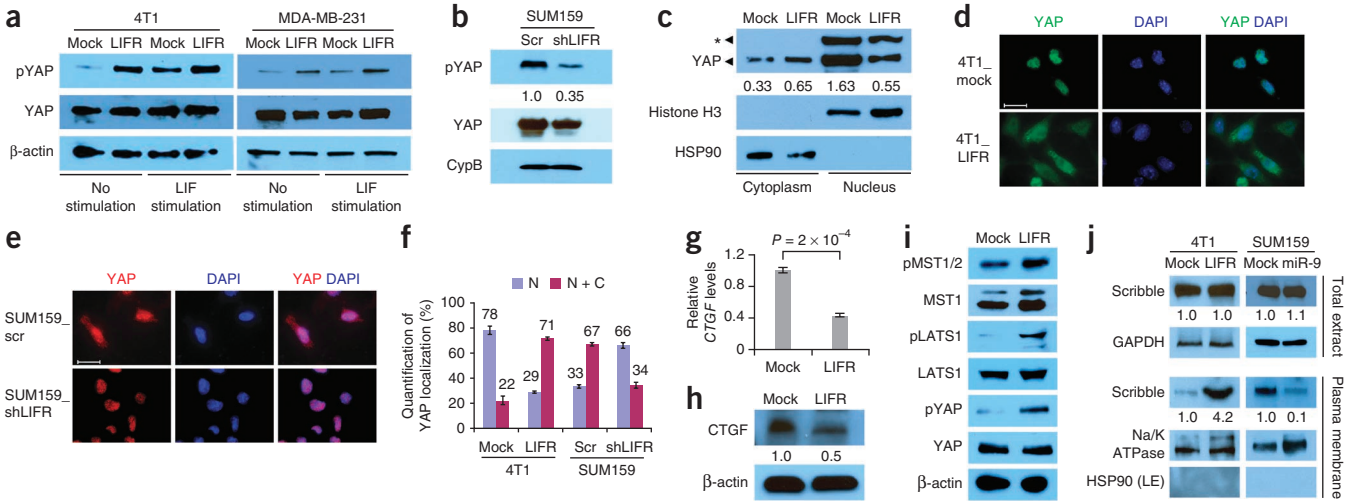


**Figure 3** LIFR activates Hippo signaling and leads to phosphorylation and functional inactivation of YAP in breast cancer cells. (**a**) Immunoblotting of phosphorylated YAP (pYAP), YAP and β-actin in mock-infected and LIFR-transduced 4T1 and MDA-MB-231 cells in the presence or absence of LIF stimulation. (**b**) Immunoblotting of pYAP, YAP and cyclophilin B (CypB) in SUM159 cells infected with LIFR shRNA (shLIFR) or the pGIPZ-GFP lentiviral vector with a scrambled sequence (Scr) that does not target any mRNA. (**c**) Immunoblotting of YAP, histone H3 (nuclear marker) and HSP90 (cytoplasmic marker) in cytoplasmic and nuclear fractions of 4T1 cells infected with the LIFR-expressing vector or empty vector (mock). The asterisk indicates a nonspecific band that is enriched in the nuclear fraction. (**d**) Immunofluorescent staining of YAP (green) in mock-infected and LIFR-transduced 4T1 cells. The images on the right are the overlay of YAP and nuclear DAPI (blue) staining of the same field. Scale bar, 20 μm. (**e**) Immunofluorescent staining of YAP (red) in SUM159 cells infected with the LIFR shRNA (SUM159_shLIFR) or the pGIPZ-GFP lentiviral vector with a scrambled sequence (SUM159_scr). The images on the right are the overlay of YAP and nuclear DAPI (blue) staining of the same field. Scale bar, 20 μm. (**f**) Percentage of cells with exclusively nuclear (N) YAP and cells with both nuclear and cytoplasmic (N + C) YAP. No cells showed YAP that was localized exclusively in the cytoplasm. Data are means ± s.e.m. ($n = 5$ fields per group). (**g**,**h**) qPCR (**g**) and immunoblot (**h**) of CTGF in 4T1 cells infected with the LIFR-expressing vector or empty vector. Data in **g** are means ± s.e.m. Statistical significance was determined by unpaired, two-tailed Student's $t$ test. (**i**) Immunoblotting of YAP upstream kinases (phosphorylated MST1 and MST2 (pMST1/2), MST1, phosphorylated LATS1 (pLATS1) and LATS1) in 4T1 cells infected with the LIFR-expressing vector or empty vector. (**j**) Immunoblotting of total Scribble and plasma membrane-localized Scribble in 4T1 cells infected with the LIFR-expressing vector or empty vector and in SUM159 cells infected with the miR-9–expressing vector or empty vector. Na/K ATPase and HSP90 are markers of the plasma membrane and cytoplasm, respectively. LE, long exposure; GAPDH, glyceraldehyde-3-phosphate dehydrogenase.



cells and LIFR-expressing cells (data not shown). Although *BDNF* has not been implicated in metastasis, *CTGF*, one of the best established YAP targets[24], was present in a breast cancer metastasis gene set[27]. Consistent with the effect on mRNA levels, expression of LIFR in 4T1 cells resulted in a 50% reduction in the level of connective tissue growth factor (CTGF) protein (**Fig. 3h**).

The Hippo-YAP pathway regulates organ size and tumorigenesis[25,26,28]. However, the cell membrane receptors that activate Hippo signaling remain elusive[25,26]. We examined the cytosolic kinases upstream of YAP: large tumor suppressor (LATS), which phosphorylates and inhibits YAP and TAZ, and MST (the mammalian Hippo homolog), which phosphorylates and activates LATS[25]. Consistent with increased YAP phosphorylation, restoring LIFR expression in 4T1 cells increased phosphorylation of MST1, MST2 and LATS1 (**Fig. 3i**), suggesting that LIFR triggers a kinase cascade that leads to phosphorylation, cytoplasmic retention and functional inactivation of YAP.

How does LIFR activate Hippo signaling? Recently, Scribble was identified as an upstream regulator of Hippo signaling: when localized at the cell membrane, Scribble serves as an adaptor to assemble a protein complex consisting of MST, LATS and YAP or TAZ and promotes this phosphorylation cascade. When localized in the cytoplasm, Scribble cannot bring MST, LATS and YAP or TAZ together[29]. In the present study, expression of LIFR in 4T1 cells did not alter the level of Scribble in total cell extracts but did lead to a pronounced enrichment of Scribble at the plasma membrane (**Fig. 3j**). On the contrary, expression of miR-9 in SUM159 cells inhibited the cell-membrane localization of Scribble (**Fig. 3j**). These data reveal a mechanistic link between LIFR and the activation of Hippo signaling (**Supplementary Discussion**).

### LIFR inhibits breast cancer metastasis by inactivating YAP

The function of YAP in metastasis has not been shown. As knockdown of LIFR in SUM159 cells reduced the inhibitory phosphorylation of YAP (**Fig. 3b**) and promoted its nuclear localization (**Fig. 3e**,**f**), we silenced YAP in these cells (**Fig. 4a**). This resulted in a complete reversion of the cell migration and invasion induced by LIFR shRNA (**Supplementary Fig. 8a**,**c**). We then intravenously injected these shRNA-expressing SUM159 cells into nude mice. At 30 d after injection, all mice bearing SUM159 cells expressing LIFR shRNA were moribund as a result of massive lung metastases (averaging 62 visible metastases per mouse; **Fig. 4b**,**c** and **Supplementary Fig. 8d**). In contrast, mice injected with control SUM159 cells (expressing a scramble shRNA) or SUM159 cells with simultaneous knockdown of LIFR and YAP (expressing LIFR shRNA and YAP shRNA) were viable and free of detectable metastases at this time point (**Fig. 4b**,**c** and **Supplementary Fig. 8d**). Therefore, loss of LIFR triggers migration, invasion and metastatic colonization through activation of YAP.

To further determine whether phosphorylation-dependent inhibition of YAP mediates the metastasis-suppressing effect of LIFR, we expressed wild-type mouse YAP, the nonphosphorylatable YAP mutant (S112A) or CTGF in LIFR-overexpressing 4T1 cells (**Fig. 4d**). Either CTGF or the S112A YAP mutant, but not wild-type YAP, reversed the inhibitory effect of LIFR on cell migration and invasion *in vitro* (**Supplementary Fig. 8b**,**e**).

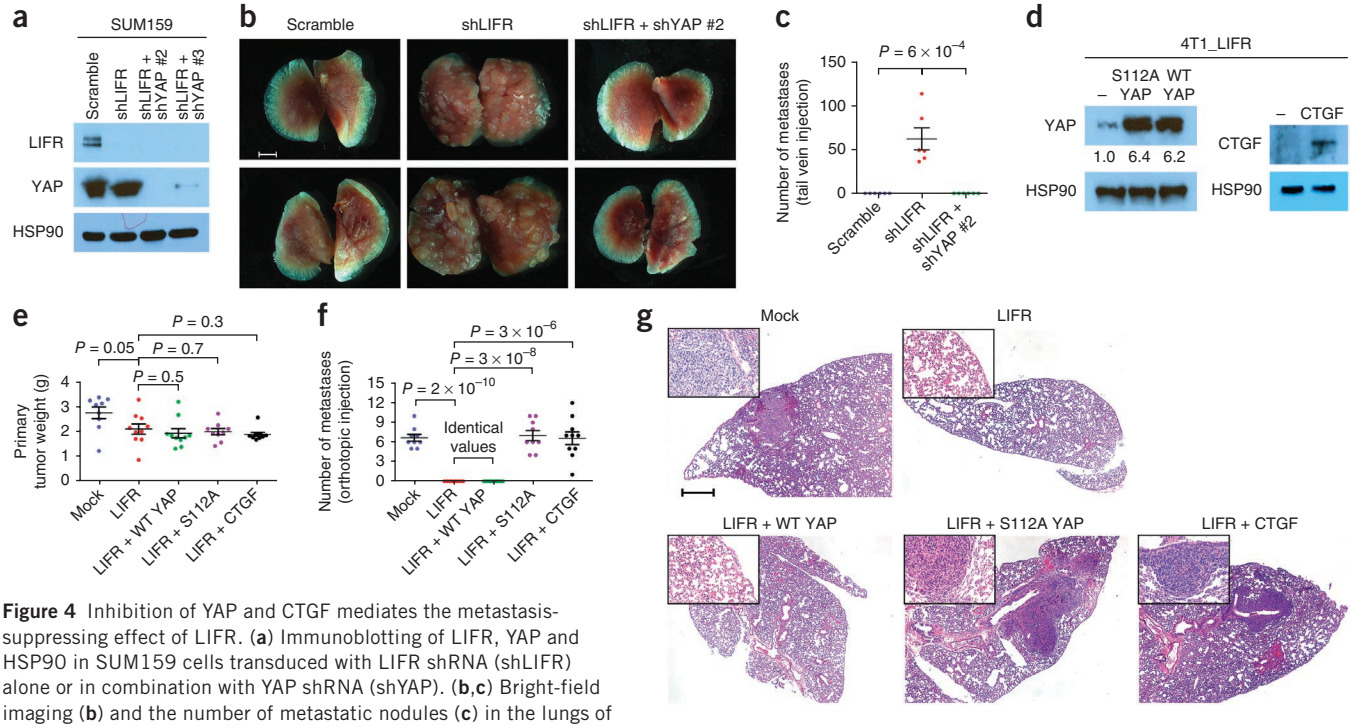


**Figure 4** Inhibition of YAP and CTGF mediates the metastasis-suppressing effect of LIFR. (**a**) Immunoblotting of LIFR, YAP and HSP90 in SUM159 cells transduced with LIFR shRNA (shLIFR) alone or in combination with YAP shRNA (shYAP). (**b**,**c**) Bright-field imaging (**b**) and the number of metastatic nodules (**c**) in the lungs of mice with tail vein injection of SUM159 cells transduced with LIFR shRNA alone or in combination with YAP shRNA at day 30 after implantation. Scale bar, 2,000 μm. Data in **c** are means ± s.e.m. ($n = 6$ mice per group). (**d**) Immunoblotting of YAP, CTGF and HSP90 in LIFR-expressing 4T1 cells transduced with wild-type (WT) YAP, the S112A YAP mutant or CTGF. (**e**,**f**) Primary mammary tumor weight (**e**) and the number of metastatic nodules in the lungs (**f**) of mice with orthotopic injection of mock-infected 4T1 cells and LIFR-expressing 4T1 cells transduced with wild-type YAP, the S112A YAP mutant or CTGF at day 22 after implantation. Metastatic nodules were counted under a stereomicroscope and subsequently verified by H&E staining. Data are means ± s.e.m. ($n = 9$, 10, 10, 9 and 10 mice, respectively, in the five groups shown from left to right). (**g**) H&E staining of lungs isolated from the mice described in **f**. Scale bar, 500 μm. Insets are high-magnification images (×200) of specific areas in the corresponding low-magnification (×25) images. Statistical significance was determined by unpaired, two-tailed Student's *t* test.

We subsequently performed orthotopic implantation experiments with these engineered 4T1 cell lines and euthanized all recipients at day 22 after implantation because of excessive mammary tumor burdens. Expression of wild-type YAP in LIFR-transduced 4T1 cells did not alter primary tumor growth (**Fig. 4e**) or rescue lung metastasis formation (**Fig. 4f**,**g**). In contrast, either CTGF or the nonphosphorylatable YAP mutant fully reversed the metastasis-suppressing effect of LIFR (**Fig. 4f**,**g**) without affecting the size of the primary tumor (**Fig. 4e**). Collectively, these data suggest that LIFR inhibits breast cancer metastasis through, at least in part, phosphorylation-dependent inactivation of YAP and its target, CTGF.

## LIFR is downregulated in human breast cancer

*LIFR* mRNA is downregulated in a variety of human cancers (**Supplementary Table 2**). We searched for *LIFR* in Oncomine[30]. In 11 of 15 cancer types, *LIFR* was downregulated in tumor tissues compared with normal tissues (**Supplementary Fig. 9a**). In breast cancer, 15 of 19 analyses, based on nine datasets, showed downregulation of *LIFR* in tumor issue compared with normal breast tissue[31–39] (**Supplementary Table 3**). Five of these nine datasets specifically compared invasive breast cancer with normal breast tissue, and *LIFR* was consistently found to be downregulated in these data[32,33,35,37,39] (**Supplementary Table 3** and **Supplementary Fig. 9b–f**).

To determine LIFR protein expression in human patients with breast cancer, we performed immunohistochemical staining of LIFR on the National Cancer Institute (NCI) Progression tissue microarrays (TMAs; Online Methods) with a LIFR-specific antibody that was validated for immunohistochemistry (**Supplementary Fig. 10**). Out of 34 total normal breast tissue samples, 32 (94%) had high expression of LIFR (**Fig. 5a** and **Supplementary Fig. 11a**,**b**). In contrast, 35% (6 of 17) of ductal carcinoma *in situ* (DCIS) specimens and 43% (57 of 134) of invasive breast carcinoma specimens had low to negative expression of LIFR (**Fig. 5a** and **Supplementary Fig. 11a–c**). Thus, LIFR protein is underexpressed in DCIS ($P = 0.006$) and invasive breast carcinoma ($P = 0.0001$) compared with normal mammary tissue.

Of the 134 individuals with invasive breast carcinoma, 114 had known status (either positive or negative) of lymph node metastasis. Forty-six patients were negative for lymph node metastasis and 33% of these patients had low to negative expression of LIFR in their breast tumors. Sixty-eight patients were positive for lymph node metastasis, and 53% of them showed downregulation or loss of LIFR (**Fig. 5a** and **Supplementary Fig. 11d**). Therefore, LIFR inversely correlates with lymph node metastasis in patients with invasive breast cancer ($P = 0.03$).

## Loss of LIFR correlates with poor clinical outcomes

LIFR did not correlate with estrogen receptor or progesterone receptor status (**Supplementary Fig. 12a**,**b**) and showed no significant difference between DCIS and invasive breast carcinoma (**Supplementary Fig. 11c**). Moreover, Oncomine analyses revealed widespread downregulation of *LIFR* in various human cancers (**Supplementary Fig. 9a**). On the basis of these data, downregulation or loss of LIFR may be an early event in tumorigenesis that contributes to progression to metastasis. However, proof of this requires further studies of LIFR in a large cohort of patients

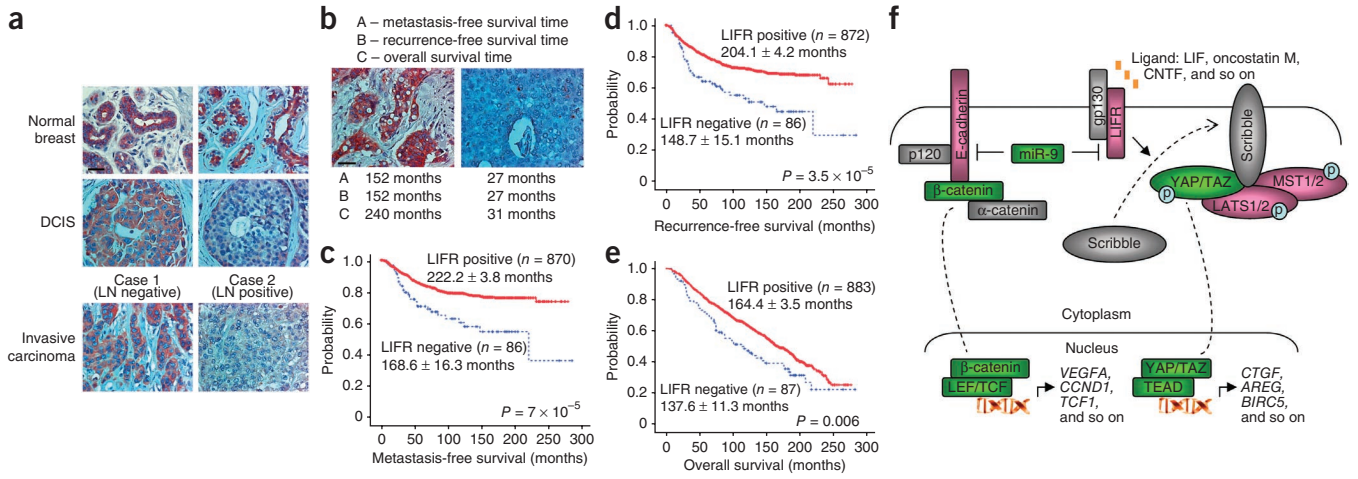


**Figure 5** LIFR is downregulated in human breast cancer and correlates with clinical outcomes. (**a**) Immunohistochemical staining of LIFR in representative normal breast, DCIS and invasive breast carcinoma specimens on the NCI Progression TMAs. Brown staining indicates LIFR immunoreactivity. Scale bar, 50 μm. LN, lymph node metastasis. (**b**) Immunohistochemical staining of LIFR in two representative breast tumor specimens (left, LIFR positive; right, LIFR negative) on the NCI Prognostic TMAs. Brown staining indicates LIFR immunoreactivity. Scale bar, 50 μm. The survival times of both patients are listed. (**c**–**e**) Kaplan-Meier graphs representing the probability of cumulative metastasis-free (free of distant metastasis) survival (**c**), recurrence-free (recurrence indicates tumor relapse at the primary site, the metastatic site or both) survival (**d**) and overall survival (**e**) in patients with breast cancer stratified according to LIFR expression status in their primary tumors. Survival time data are presented as means ± s.e.m. (mean survival time is estimated as the area under the survival curve). The log-rank test *P* value reflects the significance of the correlation between LIFR positivity and longer survival outcome. (**f**) Model of two metastasis suppressor pathways that are negatively regulated by miR-9 in breast cancer cells. Green indicates oncogenic and/or pro-metastatic factors; pink indicates tumor-suppressing and/or metastasis-suppressing factors. MST1/2, mammalian Hippo homologs 1 and 2; LEF/TCF, lymphoid enhancer-binding factor/T cell-specific factor; LATS1/2, large tumor suppressor homologs 1 and 2; TEAD, TEA domain. "p" in the circles indicates phosphorylation.

to determine whether LIFR expression status in nonmetastatic breast tumors is associated with future clinical outcomes.

To address this issue, we obtained NCI Prognostic TMAs containing 1,169 nonmetastatic breast tumor specimens that have a long-term clinical follow-up record (Online Methods), immunostained these TMAs with a LIFR-specific antibody and divided the specimens into two groups (**Fig. 5b**): LIFR positive and LIFR negative (no detectable immunoreactivity). We found loss of LIFR in 4.4%, 12.2% and 13.4% of breast tumors classified as stage I, stage II and stage III, respectively, showing a significant correlation ($P = 0.0004$) of LIFR with tumor, node, metastasis (TNM) stage (**Supplementary Fig. 12c**). Of tumors with negative and positive distant metastasis outcome, 7.3% and 15.5%, respectively, were negative for LIFR (**Supplementary Fig. 12d**); moreover, 6% of tumors with negative lymph node metastasis outcome and 13% of tumors with positive lymph node metastasis outcome lacked LIFR (**Supplementary Fig. 12e**). Therefore, loss of LIFR is associated with future development of distant metastasis ($P = 0.004$) and lymph node metastasis ($P = 0.001$).

We then performed Kaplan-Meier analyses to determine whether LIFR is a prognostic marker for clinical outcomes. Nine-hundred fifty-six patients were analyzable for metastasis-free survival, and patients with LIFR-negative tumors had a higher probability of developing future metastasis at distant sites (168.6 ± 16.3 months, mean ± s.e.m.) than those with LIFR-positive tumors (222.2 ± 3.8 months; $P = 7 \times 10^{-5}$; **Fig. 5c**). Nine-hundred fifty-eight patients were analyzable for recurrence-free survival, and patients with loss of LIFR in their tumors had shorter recurrence-free survival (148.7 ± 15.1 months) than those with positive LIFR expression (204.1 ± 4.2 months; $P = 3.5 \times 10^{-5}$; **Fig. 5d**). Nine-hundred seventy patients were analyzable for overall survival, and patients with LIFR-positive tumors had longer overall survival (164.4 ± 3.5 months) than those with tumors lacking LIFR (137.6 ± 11.3 months; $P = 0.006$; **Fig. 5e**). These data suggest the potential use of LIFR in prognostic stratification of patients with breast cancer.

## DISCUSSION

We identified LIFR as a new breast cancer metastasis suppressor that inhibits both local invasion and metastatic colonization. Although LIFR expression did not substantially affect the size of the primary tumors formed by the aggressive breast cancer cells used in this study (except to cause an initial delay in 4T1 tumor growth), whether LIFR regulates primary tumor formation should be determined by loss-of-function analyses of LIFR in preneoplastic cells (**Supplementary Discussion**). Notably, LIFR is highly relevant in human tumors: although 94% of normal breast tissues have high LIFR expression, this protein is downregulated or lost in a significant fraction of patients with DCIS or invasive breast cancer and is inversely associated with lymph node metastasis in patients with invasive breast carcinoma. Significantly, tumors with loss of LIFR correlated with poor prognosis in approximately 1,000 women with nonmetastatic stage I–III breast cancer.

We found that LIFR functions through the Hippo-YAP pathway to suppress metastasis. Whereas a conserved Hippo kinase cascade has been established in *Drosophila* and mammals, the cell membrane receptors that activate Hippo signaling remain elusive[25,26]. Our findings show that LIFR alters Scribble localization and activates the MST-LATS-YAP phosphorylation cascade. Taken together with previous findings, miR-9 can target two alternative metastasis suppressors, LIFR and E-cadherin (**Fig. 5f**); whereas E-cadherin maintains adherens junctions and sequesters β-catenin at the cytoplasmic membrane, LIFR promotes localization of Scribble to the cell membrane, which in turn activates Hippo signaling, leading to the phosphorylation and functional inactivation of the transcriptional coactivator YAP. Additional metastasis genes regulated by LIFR (**Supplementary Fig. 13** and **Supplementary Discussion**) remain to be investigated.

From The Cancer Genome Atlas (TCGA) breast cancer data, both mir-9-1 and mir-9-2 have a moderate but significant inverse correlation with *LIFR* (**Supplementary Fig. 14a**,**b** and **Supplementary Discussion**), suggesting that LIFR can be suppressed by miR-9, as well as other mechanisms. The expression levels of *LIFR* and *IL6ST* (encoding the co-receptor gp130) were positively correlated in human breast tumors (**Supplementary Fig. 15a**). Moreover, knockdown of gp130 reversed LIFR-induced YAP phosphorylation (**Supplementary Fig. 15b**), whereas LIF stimulation recapitulated the effect of LIFR on YAP phosphorylation in breast cancer cells. These results suggest that the co-receptor (gp130) and the ligand (LIF) may be involved in LIFR-induced cell-membrane localization of Scribble and subsequent activation of the Hippo phosphorylation cascade (**Supplementary Discussion**).

Until recently, only a few metastasis suppressor genes had been identified[4,5]. Aided by the rapid development and widespread availability of new technologies and experimental systems, this field has been growing in the past few years, leading to an expansion of the list of potential metastasis suppressor genes from only a few to at least 23 (ref. 40). Elevating the expression of metastasis suppressor proteins has been useful preclinically and in clinical trials[40]. We envision that therapeutic intervention centered on restoring LIFR expression or function could be useful for blocking breast cancer metastasis.

## METHODS

Methods and any associated references are available in the online version of the paper.

*Note: Supplementary information is available in the online version of the paper.*

### ACKNOWLEDGMENTS

We are grateful to R.A. Weinberg for his advice and reagents. We thank S. Ethier for providing cell lines; F. Reinhardt for advice on mouse surgery; the Genome Technology Core at the Whitehead Institute, the ShRNA and ORFeome Core at MD Anderson Cancer Center and the Histology Core Laboratories at MD Anderson Cancer Center and Memorial Sloan-Kettering Cancer Center for technical assistance; and members of the Ma Lab for discussion. We thank J. Chen, K. Muller, W. Pagel, K. Keyomarsi, L. Li and R. Cleveland for critical reading of the manuscript. This work is supported by the US National Institutes of Health grants R00CA138572 (to L.M.), R01CA166051 (to L.M.), R01CA109311 (to M.-C.H.) and P01CA099031 (to M.-C.H.), a Cancer Prevention and Research Institute of Texas Scholar Award R1004 (to L.M.), a University of Texas STARS Award (to L.M.), a Faculty Development Award (to L.M.) from the MD Anderson Cancer Center Support grant CA016672 from the US National Institutes of Health, Center for Biological Pathways (to Y.S. and M.-C.H.), a Susan G. Komen for the Cure grant SAC110016 (to M.-C.H.), the National Breast Cancer Foundation, Inc. and the Sister Institution Fund of China Medical University and Hospital and MD Anderson Cancer Center (to M.-C.H.).

### AUTHOR CONTRIBUTIONS

L.M. conceived of and supervised the project. D.C. and L.M. designed, performed and analyzed most of the experiments. Y.S. maintained shRNA and open reading frame (ORF) libraries, constructed RNA-Seq libraries and analyzed RNA-Seq data. Y.W. and M.-C.H. performed studies on tissue microarrays of human patient samples. P.Z. performed some biochemical work. A.H.R. and H.-K.L. performed tail vein injection experiments. J.T.-F. performed histopathological analysis. S.G. processed the raw data from the Solexa sequencer. H.L. performed TCGA data analysis. L.M. wrote the manuscript with input from all other authors.

### COMPETING FINANCIAL INTERESTS

The authors declare no competing financial interests.

Published online at http://www.nature.com/doifinder/10.1038/nm.2940.
Reprints and permissions information is available online at http://www.nature.com/reprints/index.html.

1. Lee, Y.T. Breast carcinoma: pattern of metastasis at autopsy. *J. Surg. Oncol.* **23**, 175–180 (1983).
2. Weigelt, B., Peterse, J.L. & van 't Veer, L.J. Breast cancer metastasis: markers and models. *Nat. Rev. Cancer* **5**, 591–602 (2005).
3. Steeg, P.S. Tumor metastasis: mechanistic insights and clinical challenges. *Nat. Med.* **12**, 895–904 (2006).
4. Steeg, P.S. & Theodorescu, D. Metastasis: a therapeutic target for cancer. *Nat. Clin. Pract. Oncol.* **5**, 206–219 (2008).
5. Vaidya, K.S. & Welch, D.R. Metastasis suppressors and their roles in breast carcinoma. *J. Mammary Gland Biol. Neoplasia* **12**, 175–190 (2007).
6. Bartel, D.P. MicroRNAs: genomics, biogenesis, mechanism, and function. *Cell* **116**, 281–297 (2004).
7. He, L. & Hannon, G.J. MicroRNAs: small RNAs with a big role in gene regulation. *Nat. Rev. Genet.* **5**, 522–531 (2004).
8. Bartel, D.P. MicroRNAs: target recognition and regulatory functions. *Cell* **136**, 215–233 (2009).
9. Nicoloso, M.S., Spizzo, R., Shimizu, M., Rossi, S. & Calin, G.A. MicroRNAs—the micro steering wheel of tumour metastases. *Nat. Rev. Cancer* **9**, 293–302 (2009).
10. Ma, L., Teruya-Feldstein, J. & Weinberg, R.A. Tumour invasion and metastasis initiated by microRNA-10b in breast cancer. *Nature* **449**, 682–688 (2007).
11. Tavazoie, S.F. *et al.* Endogenous human microRNAs that suppress breast cancer metastasis. *Nature* **451**, 147–152 (2008).
12. Huang, Q. *et al.* The microRNAs miR-373 and miR-520c promote tumour invasion and metastasis. *Nat. Cell Biol.* **10**, 202–210 (2008).
13. Valastyan, S. *et al.* A pleiotropically acting microRNA, miR-31, inhibits breast cancer metastasis. *Cell* **137**, 1032–1046 (2009).
14. Ma, L. *et al.* miR-9, a MYC/MYCN-activated microRNA, regulates E-cadherin and cancer metastasis. *Nat. Cell Biol.* **12**, 247–256 (2010).
15. Ma, L. *et al.* Therapeutic silencing of miR-10b inhibits metastasis in a mouse mammary tumor model. *Nat. Biotechnol.* **28**, 341–347 (2010).
16. Huntsman, D.G. *et al.* Early gastric cancer in young, asymptomatic carriers of germ-line E-cadherin mutations. *N. Engl. J. Med.* **344**, 1904–1909 (2001).
17. Chan, J.K. & Wong, C.S. Loss of E-cadherin is the fundamental defect in diffuse-type gastric carcinoma and infiltrating lobular carcinoma of the breast. *Adv. Anat. Pathol.* **8**, 165–172 (2001).
18. Lewis, B.P., Burge, C.B. & Bartel, D.P. Conserved seed pairing, often flanked by adenosines, indicates that thousands of human genes are microRNA targets. *Cell* **120**, 15–20 (2005).
19. Gearing, D.P. The leukemia inhibitory factor and its receptor. *Adv. Immunol.* **53**, 31–58 (1993).
20. Kishimoto, T., Akira, S., Narazaki, M. & Taga, T. Interleukin-6 family of cytokines and gp130. *Blood* **86**, 1243–1254 (1995).
21. Tamm, C., Bower, N. & Anneren, C. Regulation of mouse embryonic stem cell self-renewal by a Yes-YAP-TEAD2 signaling pathway downstream of LIF. *J. Cell Sci.* **124**, 1136–1144 (2011).
22. Zhao, B. *et al.* Angiomotin is a novel Hippo pathway component that inhibits YAP oncoprotein. *Genes Dev.* **25**, 51–63 (2011).
23. Zhao, B. *et al.* Inactivation of YAP oncoprotein by the Hippo pathway is involved in cell contact inhibition and tissue growth control. *Genes Dev.* **21**, 2747–2761 (2007).
24. Zhao, B. *et al.* TEAD mediates YAP-dependent gene induction and growth control. *Genes Dev.* **22**, 1962–1971 (2008).
25. Zhao, B., Li, L., Lei, Q. & Guan, K.L. The Hippo-YAP pathway in organ size control and tumorigenesis: an updated version. *Genes Dev.* **24**, 862–874 (2010).
26. Pan, D. The hippo signaling pathway in development and cancer. *Dev. Cell* **19**, 491–505 (2010).
27. Kang, Y. *et al.* A multigenic program mediating breast cancer metastasis to bone. *Cancer Cell* **3**, 537–549 (2003).
28. Dong, J. *et al.* Elucidation of a universal size-control mechanism in *Drosophila* and mammals. *Cell* **130**, 1120–1133 (2007).
29. Cordenonsi, M. *et al.* The Hippo transducer TAZ confers cancer stem cell–related traits on breast cancer cells. *Cell* **147**, 759–772 (2011).
30. Rhodes, D.R. *et al.* ONCOMINE: a cancer microarray database and integrated data-mining platform. *Neoplasia* **6**, 1–6 (2004).
31. Richardson, A.L. *et al.* X chromosomal abnormalities in basal-like human breast cancer. *Cancer Cell* **9**, 121–132 (2006).
32. Zhao, H. *et al.* Different gene expression patterns in invasive lobular and ductal carcinomas of the breast. *Mol. Biol. Cell* **15**, 2523–2536 (2004).
33. Finak, G. *et al.* Stromal gene expression predicts clinical outcome in breast cancer. *Nat. Med.* **14**, 518–527 (2008).
34. Sørlie, T. *et al.* Gene expression patterns of breast carcinomas distinguish tumor subclasses with clinical implications. *Proc. Natl. Acad. Sci. USA* **98**, 10869–10874 (2001).
35. Radvanyi, L. *et al.* The gene associated with trichorhinophalangeal syndrome in humans is overexpressed in breast cancer. *Proc. Natl. Acad. Sci. USA* **102**, 11005–11010 (2005).
36. Sorlie, T. *et al.* Repeated observation of breast tumor subtypes in independent gene expression data sets. *Proc. Natl. Acad. Sci. USA* **100**, 8418–8423 (2003).
37. Turashvili, G. *et al.* Novel markers for differentiation of lobular and ductal invasive breast carcinomas by laser microdissection and microarray analysis. *BMC Cancer* **7**, 55 (2007).
38. Perou, C.M. *et al.* Molecular portraits of human breast tumours. *Nature* **406**, 747–752 (2000).
39. Karnoub, A.E. *et al.* Mesenchymal stem cells within tumour stroma promote breast cancer metastasis. *Nature* **449**, 557–563 (2007).
40. Smith, S.C. & Theodorescu, D. Learning therapeutic lessons from metastasis suppressor proteins. *Nat. Rev. Cancer* **9**, 253–264 (2009).

## ONLINE METHODS

**Cell culture.** The MCF7, T47D, MDA-MB-231, 4T1 and 293T cell lines were purchased from American Type Culture Collection and were cultured under conditions specified by the manufacturer. The SUM149, SUM159, SUM229 and SUM1315 cell lines were from S. Ethier and cultured as described (SUM149, SUM159 and SUM229 cell lines, http://www.asterand.com/Asterand/human_tissues/149PT.htm; SUM1315 cell line, http://www.asterand.com/Asterand/human_tissues/1315M02.htm). Mouse and human LIF ligands were purchased from Gibco and Millipore, respectively. For LIF stimulation, cells were starved in serum-free medium and then treated with mouse (for 4T1 cells, 10 ng/ml for 30 min) or human (for MDA-MB-231 cells, 50 ng/ml for 1 h) LIF, according to the manufacturer's instructions.

**Plasmids and shRNA.** The human *mir-9-3* genomic sequence was PCR amplified from normal genomic DNA and cloned into the MDH1-PGK-GFP 2.0 retroviral vector as previously described[14]. A *LIFR* 3′ UTR fragment (801 bp) was cloned into the pMIR-REPORT luciferase construct[10] using the following cloning primers: forward, 5′-TGCACACTAGTCAGTGTCACCGTGTCACTTCA-3′; reverse, 5′-CTAGTAAGCTTGTCTCTAGTCTTAGAAGTGTA-3′. The shRNA and ORF clones were from Open Biosystems through MD Anderson's ShRNA and ORFeome Core, and the clone numbers are as follows: human LIFR shRNA, V3LHS-347493 (designated as 'A8') and V3LHS-347496 (designated as 'F3'); human YAP shRNA, V2LHS_65508 and V3LHS-306101; mouse gp130 shRNA, V2LMM-219118 and V3LMM-503552; human LIFR ORF, PLOH-100016429; mouse LIFR fully sequenced complementary DNA (cDNA), 4159053; mouse YAP ORF, MMM1013-7510984; and mouse CTGF ORF, MMM1013-64071. The shRNA sequences can be found at https://www.openbiosystems.com/ using the clone numbers. The LIFR 3′ UTR mutant and the YAP nonphosphorylatable mutant were generated using a QuikChange Site-Directed Mutagenesis Kit (Stratagene). The vectors used in this study are listed in **Supplementary Table 4**.

**siRNA oligonucleotides.** Four individual siRNAs that target human *LIFR* were purchased from Sigma and Dharmacon. The siRNA sequences are as follows: (i) GUUGCAAUCAAGAUUCGUA (Sigma, SASI_Hs02_00330115); (ii) CGAUUAACAGUGUCACCGU (Sigma, SASI_Hs02_00330118); (iii) CCA CACCGCUCAAAUGUUA (Dharmacon, J-008017-06); and (iv) GAAC AAAACGUUUCCUUAA (Dharmacon, J-008017-08). Cells were transfected with 150 nM of the indicated oligonucleotide using the Oligofectamine reagent (Invitrogen). Forty-eight hours after transfection, cells were plated for migration and invasion assays, and the remaining cells were harvested for western blot analysis.

**RNA isolation and real-time RT-PCR.** Total RNA, with efficient recovery of small RNAs, was isolated using the mirVana miRNA Isolation Kit (Ambion) and was then reverse transcribed with an iScript cDNA Synthesis Kit (Bio-Rad). The resulting cDNA was used for qPCR using the TaqMan Gene Expression Assays (Applied Biosystems), and data were normalized to an endogenous control, β-actin. Quantification of the mature form of the miRNAs was performed using the TaqMan MicroRNA Assay Kit (Applied Biosystems) according to the manufacturer's instructions, and U6 small nuclear RNA was used as an internal control. Real-time PCR and data collection were performed on a CFX96 instrument (Bio-Rad).

**Tumor metastasis PCR array analysis.** The Tumor Metastasis RT$^2$ Profiler PCR Array, consisting of 84 genes known to be involved in metastasis, was used to profile LIFR-expressing 4T1 cells according to the manufacturer's instructions (http://www.sabiosciences.com/rt_pcr_product/HTML/PAMM-028Z.html). Briefly, total RNA was extracted and reverse transcribed into cDNA using an RT$^2$ First Strand Kit (Qiagen). The cDNA was combined with an RT$^2$ SYBR Green qPCR Master Mix (Qiagen), and then equal aliquots of this mixture (25 µl) were added to each well of the same PCR Array plate that contained the predispensed gene-specific primer sets. Real-time PCR and data collection were performed on a CFX96 instrument (Bio-Rad).

**Lentiviral and retroviral transduction.** The production of lentivirus and amphotropic retrovirus and the infection of target cells were performed as described previously[41].

**miRNA target analysis.** Genes that contained the miR-9–binding site(s) in their 3′ UTR were obtained using the TargetScan program[18] (http://www.targetscan.org/; version 5.1). The RNAhybrid program[42] was used to predict duplex formation between human *LIFR* 3′ UTR and miR-9.

**Cell growth and viability assays.** To determine growth curves, we plated equal numbers of cells in 6-cm dishes. Beginning the next day, cells were trypsinized and counted every day. To determine cell viability, we trypsinized cells and diluted them with 0.4% trypan blue staining solution. Cell counts and the percentages of viable cells were obtained from a TC10 Automated Cell Counter (Bio-Rad).

**Migration and invasion assays.** Transwell migration and Matrigel invasion assays were performed as described previously[10].

**Luciferase reporter assay.** Dual luciferase reporter assays were performed as described previously[10].

**Immunoblotting.** Western blot analyses were performed with precast gradient gels (Bio-Rad) using standard methods. Briefly, cells were lysed in the radioimmunoprecipitation assay (RIPA) buffer containing protease inhibitors (Roche) and phosphatase inhibitors (Sigma). Proteins were separated by SDS-PAGE and blotted onto a nitrocellulose membrane (Bio-Rad). Membranes were probed with the specific primary antibodies and then with peroxidase-conjugated secondary antibodies. The bands were visualized by chemiluminescence (Denville Scientific). The following antibodies were used: antibodies to LIFR (1:1,000, Santa Cruz Biotechnology, sc-659), gp130 (1:500, Upstate, 09-261), E-cadherin (1:1,000, BD Transduction Laboratories, 610182), pSTAT3 (phosphorylated at Tyr705; 1:1,000, Cell Signaling Technology, 9131), STAT3 (1:1,000, Cell Signaling Technology, 9132), pYAP (Ser127; 1:1,000, Cell Signaling Technology, 4911), YAP (1:500, Cell Signaling Technology, 4912), pLATS1 (Ser909; 1:500, Cell Signaling Technology, 9157), LATS1 (1:1,000, Cell Signaling Technology, 3477), pMST1 (Thr183)/MST2 (Thr180) (1:500, Cell Signaling Technology, 3681), MST1 (1:500, Cell Signaling Technology, 3682), histone H3 (1:1,000, Millipore, 06-755), HSP90 (1:3,000, BD Transduction Laboratories, 610419), CTGF (1:500, Abcam, ab6992; and 1:500, Santa Cruz Biotechnology, sc-34772), Scribble (1:500, Santa Cruz Biotechnology, sc-11048), Na/K ATPase (1:500, Santa Cruz Biotechnology, sc-21712), vimentin (1:2,000, NeoMarkers, MS-129-P), β-actin (1:5,000, Sigma, A5441), cyclophilin B (1:2,000, Thermo, PA1-027A) and GAPDH (1:3,000, Thermo, MA5-15738). The ImageJ program (http://rsbweb.nih.gov/ij/download.html) was used for densitometric analyses of western blots, and the quantification results were normalized to the loading control.

**Fractionation.** Fractionation of nuclear and cytoplasmic proteins was done using the NE-PER Nuclear and Cytoplasmic Extraction Kit (Thermo) according to the manufacturer's protocol. After fractionation, 30 µg of protein was used for western blot analysis of YAP in the cytoplasm and nucleus. HSP90 and histone H3 were used as markers of cytoplasm and the nucleus, respectively. Plasma membrane proteins were isolated using the Plasma Membrane Protein Extraction Kit (Abcam) according to the manufacturer's protocol. Twenty-five micrograms of protein was used for the western blot analysis of plasma-membrane–localized Scribble. HSP90 and Na/K ATPase were used as markers of cytoplasm and the plasma membrane, respectively.

**Immunofluorescence.** Cells were cultured in chamber slides overnight and fixed with 3.7% formaldehyde in PBS for 20 min at 4 °C and then permeabilized with 0.5% Triton X-100 in PBS for 30 min. Cells were then blocked for nonspecific binding with 5% milk in PBS and Tween-20 (PBST) overnight and incubated with YAP-specific antibody (1:300, Cell Signaling Technology, 4912) at 37 °C for 1 h and then incubated with Alexa Fluor 488 goat anti-rabbit IgG (1:500, Invitrogen, A11008) or Alexa Fluor 594 goat anti-rabbit IgG (1:500, Invitrogen, A11012) at 37 °C for 1 h. Cover slips were mounted on slides using antifade mounting medium with DAPI. Immunofluorescence images were acquired on a Zeiss Axio Observer Z1 microscope.

**RNA sequencing analysis.** Ten micrograms of total RNA from each sample was used to construct RNA-Seq libraries using the Solexa kit (Illumina) according




doi:10.1038/nm.2940

to the manufacturer's instructions. Images acquired from the Solexa sequencer were processed through the bundled Solexa image extraction pipeline version 1.6. RNA-Seq reads were aligned to the human reference sequence NCBI Build 36.1 (hg18) using ELAND (as implemented in CASAVA version 1.6). Briefly, the first 25 bases of a read were used as a seed. Each matched seed was then extended to 36 bases and scored to break any ties between multimatches. For mRNA expression counts, unique reads in the genome that landed within any exons of NCBI gene models (v37.1) were counted. The counts were normalized to the mRNA length and then further normalized to one million total reads to obtain the reads per kilobase of exon per million mapped reads (RPKM) values. The RPKM value was considered the final expression of a given sample. A list of genes ('list A') was determined by the following criteria: (i) the count of a gene was more than 1.5 times higher in mock-infected cells (SUM159_MDH1) than in miR-9–expressing SUM159 cells (SUM159_miR-9); and (ii) the count was no less than five in the SUM159_MDH1 sample. A second list of genes ('list B') that contain the miR-9 binding site(s) was obtained using the TargetScan program (http://www.targetscan.org/; version 5.1). Genes that contain miR-9–binding site(s) and are downregulated by miR-9 ('list C') were then determined by comparing list A to list B.

**Animal study.** All animal experiments were performed in accordance with a protocol approved by the Institutional Animal Care and Use Committee of MD Anderson Cancer Center. Six- to eight-week-old female NOD-SCID (for orthotopic injection of human cells), nude (for intravenous injection of human cells) or BALB/c (for all injections of mouse cells) mice were used for tumor cell implantation. For orthotopic injection, mice were anesthetized, and the skin was incised; tumor cells ($0.5 \times 10^6$) in 25 µl growth medium (mixed with Matrigel at a 1:1 ratio) were injected into the inguinal mammary fat pad using a 100-µl Hamilton microliter syringe, and the incision was then closed using wound clips. For intravenous injection, mice were placed in a restrainer, and tumor cells (4T1 cells, $0.5 \times 10^6$ cells in 100 µl PBS; SUM159 cells, $2 \times 10^6$ cells in 200 µl PBS) were injected through the tail vein using a 1-ml syringe. Mice were euthanized when they met the institutional euthanasia criteria for tumor size and overall health condition. The mammary tumors were removed and weighed; the freshly dissected primary tumors, lungs, livers, spleens, kidneys and macroscopic metastases were examined and photographed using a Zeiss SteREO Discovery V20 stereomicroscope equipped with bright-field and fluorescence imaging. Tissue samples were fixed in 10% buffered formalin overnight and then washed with PBS, transferred to 70% ethanol and then embedded in paraffin, sectioned and stained with H&E. The immunohistochemistry detection using the GFP-specific (1:1,000, Invitrogen, A6455) and vimentin-specific (human specific, 1:2,000, Dako, M0725) antibodies was performed on paraffin sections in the Histology Core Lab at Memorial Sloan-Kettering Cancer Center. Stained sections were photographed using a Zeiss Axio Observer Z1 microscope.

**Patient study.** All TMAs were purchased from the NCI Cancer Diagnosis Program. These TMAs have associated pathological and clinical outcome data from the Cooperative Breast Cancer Tissue Resource (CBCTR). The Progression TMAs consist of three different case sets, including 134 analyzable cases of invasive breast carcinoma, 17 analyzable cases of DCIS and 34 analyzable cases of normal breast tissue. The Prognostic TMAs consist of five nonoverlapping stage I case sets (590 specimens), four stage II case sets (398 specimens) and two stage III case sets (181 specimens); these nonmetastatic stage I–III breast tumor specimens have a long-term clinical follow-up record (mean follow-up time of 122 months; longest follow-up time of 284 months). Samples were deparaffinized and rehydrated. Antigen retrieval was done using 0.01 M sodium-citrate buffer (pH 6.0) in a microwave oven. To block endogenous peroxidase activity, the sections were treated with 1% hydrogen peroxide in methanol for 30 min. After 1 h of preincubation in 10% normal serum to prevent nonspecific staining, the samples were incubated with LIFR-specific antibody (1:1,500, Santa Cruz Biotechnology, sc-659) at 4 °C overnight. The sections were then treated with a biotinylated secondary antibody (Vector Laboratories, PK-6101, 1:200) and then incubated with avidin-biotin peroxidase complex solution (1:100) for 1 h at room temperature. Color was developed with the 3-amino-9-ethylcarbazole (AEC) solution. Counterstaining was carried out using Mayer's haematoxylin. All immunostained slides were scanned on the Automated Cellular Image System III (ACIS III, Dako, Denmark) for quantification by digital image analysis. A total score of protein expression was calculated from both the percentage of immunopositive cells and the immunostaining intensity. High and low protein expression were defined using the mean score of all samples as a cutoff point. Negative expression indicated no detectable immunoreactivity. Spearman rank correlation was used for statistical analyses of the correlation between LIFR and the clinical parameters. Kaplan-Meier survival analysis and the log-rank test were used for statistical analyses of the correlation between LIFR and clinical survival outcomes.

**Oncomine analysis.** Oncomine's gene search function (https://www.oncomine.org/resource/login.html) was used to assess and visualize the differential expression of a selected gene across all available datasets (updated March 2011). We searched for *LIFR* in human cancer using the following threshold values: *P* value of 0.05, fold change of 2 and gene rank in the top 10% among all differentially expressed genes. Oncomine then listed all differential expression analyses in which *LIFR* was included. For each listed analysis, the statistical results were provided and linked to graphical representations of the original microarray dataset.

**TCGA data analysis.** We obtained mRNA and miRNA expression data of clinical breast cancer from the TCGA data portal (http://cancergenome.nih.gov/). mRNA expression was measured using the Agilent 244K Custom Gene Expression G4502A-07-3 platform, and miRNA expression was measured using the Illumina (Genome Analyzer or HiSeq 2000) miRNA sequencing platform. We used the level three data provided by TCGA: log2 scale normalized data for mRNA expression, and 'reads per million miRNA reads' for miRNA expression. There are 536 tumor samples with available mRNA expression data (updated July 2011), 788 tumor samples with available miRNA expression data (updated October 2011) and 512 samples with both mRNA and miRNA expression data. Among the three precursors of miR-9 (mir-9-1, mir-9-2 and mir-9-3), the expression data of mir-9-3 in the vast majority of the samples were zero and were therefore excluded from further analyses. Spearman rank correlation was used to quantify the correlation of any miRNA-mRNA or mRNA-mRNA pair.

**Statistical analyses.** Unless otherwise noted, each sample was assayed in triplicate. Each *in vitro* experiment was repeated three to five times or more, and each *in vivo* experiment was repeated two or three times. Unless otherwise noted, data are presented as means ± s.e.m., and Student's *t* test (unpaired, two-tailed) was used to compare two groups of independent samples. Correlations of LIFR with clinical parameters and correlation of miRNA-mRNA and mRNA-mRNA pairs were analyzed using Spearman rank correlation tests. The log-rank test was used to compare Kaplan-Meier survival curves.

41. Stewart, S.A. *et al.* Lentivirus-delivered stable gene silencing by RNAi in primary cells. *RNA* **9**, 493–501 (2003).
42. Rehmsmeier, M., Steffen, P., Hochsmann, M. & Giegerich, R. Fast and effective prediction of microRNA/target duplexes. *RNA* **10**, 1507–1517 (2004).